Comparison of high-field and low-field magnetic resonance images of cadaver limbs of horses

R. C. Murray, T. S. Mair, C. E. Sherlock, A. S. Blunden

Eleven limbs taken postmortem from 10 lame horses were examined by MRI in a low-field 0·27T system designed for standing horses and a high-field 1·5T system used to examine anaesthetised horses. Nine limbs were examined in the foot/pastern region and two in the fetlock region, and the results were compared with gross pathological examinations and histological examinations of selected tissues. The appearance of normal tissues was similar between the two systems, but the anatomical arrangement of the structures was different due to differences in positioning, and a magic angle artefact was observed at different sites in some imaging sequences. Articular cartilage could be differentiated into two articular surfaces in most joints in the high-field images but could generally be separated only at the joint margins in the low-field images. Abnormalities of tendon, ligament and bone detected by gross examination were detected by both forms of MRI, but some details were clearer on the high-field images. Articular cartilage found to be normal on pathological examination was also classified as normal on MRI, but lesions in articular cartilage detected on pathological examination were identified only by high-field MRI. An abnormality was detected on MRI of all the limbs that had abnormal navicular flexor fibrocartilage on pathological examination.

Veterinary Record (2009) **165,** 281-288

R. C. Murray, MA, VetMB, MS, DipECVS, DipACVS, PhD, MRCVS,
A. S. Blunden, BVetMed, PhD, MRCPath, MRCVS,
Animal Health Trust, Lanwades Park, Kentford, Newmarket CB8 7UU

T. S. Mair, BVSc, PhD, DipECEIM, EIM, DESTS, MRCVS,
C. E. Sherlock, BVetMed, MRCVS,
Bell Equine Veterinary Clinic, Mereworth, Maidstone, Kent ME18 5GS

Correspondence to Dr Mair, e-mail: tim.mair@btinternet.com

NINETY-FIVE per cent of forelimb lameness in horses can be attributed to pain in the lower limb (Adams 1957, Ross 2003). Conventional imaging techniques have limitations in the evaluation of this region, and MRI is increasingly being used to diagnose the causes of lameness.

High-field MRI has been demonstrated to be an excellent tool for the detection of abnormalities in the feet of horses (Schramme and others 2001, Dyson and others 2003a, b, 2004, 2005, Schneider and others 2003, Dyson and Murray 2004, Kristoffersen and others 2004, Zubrod and others 2004, Boado and others 2005, Murray and Mair 2005, Blunden and others 2006a, b, Murray and others 2006a, b), and can be used to evaluate the limb up to and including the carpus and tarsus. However, although most published work has been done using high-field MRI systems designed for human beings, the expense and size of high-field units limit their use to specialist centres. A standing low-field MRI system has been available since 2002, and is potentially affordable and practical for use in clinical practice (Mair and others 2003, 2005). Initial studies using the low-field unit have revealed a similar range of lesions as those revealed by high-field scanners (Mair and others 2003, Kinns and Mair 2005, Mair and Kinns 2005, Sherlock and others 2007).

Many factors can affect the quality of MR images, and it is important to understand the characteristics, benefits and limitations of each system for the interpretation of the images of horses' limbs and for the diagnosis of lesions that result in lameness. One of these factors is the field strength of the magnets. High-field magnets have a better signal-to-noise ratio and should produce images with better resolution, which could improve the identification of small and low-contrast lesions compared with low-field magnets. Several studies have compared the results of high-field MRI with the gross and histopathological changes observed in the limbs of lame horses (Schramme and others 2005, Zubrod and others 2005, Murray and others 2006a, b, Dyson and others 2008), but no similar comparisons of low-field imaging with pathology, or of high-field with low-field MRI of the same limbs, have been published. This paper describes the characteristics of the images acquired from the same cadaver limbs of 10 lame horses by using a high-field and a low-field MRI system and compares the images for the detection of common lesions.

Materials and methods

Eleven limbs were examined from 10 randomly selected lame horses that had been euthanased for clinical reasons (Table 1). The lameness had been localised within 24 hours before the horses were euthanased, and these regions were examined by MRI. The limbs were stored frozen at –20°C in sealed plastic bags until they were examined.

Image acquisition

The limbs were thawed for 24 hours before they were imaged. The low-field images were acquired with a 0·27 T standing MRI unit (Hallmarq Veterinary Imaging). Gradient echo, fast spin echo and short tau inversion recovery (STIR) sequences were acquired in three planes: sagittal, dorsal and transverse (Table 2). A radiofrequency solenoid coil was used

TABLE 1: Characteristics of 10 horses and the pathological findings observed in the limbs that were studied

Horse	Age (years), breed, sex	Limb	Region of interest	Summary of pathological findings
1	13, Haflinger, G	LF	Foot	Evidence of penetrating wound with a necrotic tract from the lateral heel bulb to the navicular bursa; severe necrosis of DDFT with rupture/shedding of tendon lateral>medial; navicular bone fibrocartilage abnormal, especially midline to lateral; arthropathy of distal aspect of middle phalanx
2	5, Warmblood cross, F	RF	Fetlock	Complete rupture of medial collateral ligament and partial rupture of LCL, and rupture of medial joint capsule; articular cartilage damage on distal third metacarpal and proximal phalanx especially on lateral aspect; damage to distal sesamoidean ligaments
3	2, Pony, G	LF	Foot	Dorsal soft tissue damage and disruption with periosteal irregularity and thickening overlying bone damage and necrosis; common digital extensor tendon and DSIL abnormal
4	4, Hanoverian cross, G	RH	Foot/pastern	Lateral condylar fracture of middle phalanx with partial rupture of the lateral collateral ligament and complete rupture of the DSIL; loss of articular cartilage on the mid to lateral aspect of the articular surface of the distal phalanx
5	2, Warmblood, G	LF	Foot	Emaciated horse with history of malabsorption; evidence of medullary fat atrophy/necrosis, interstitial oedema and capillary infiltration; medial palmar arthrosis of distal aspect of middle phalanx
6	8, Warmblood, G	LF	Foot	Full-depth cartilage defect and underlying subchondral bone irregularity on dorsal aspect of the articular surface of the distal phalanx approximately 5 mm in diameter; partial thickness cartilage erosion on the distal aspect of the middle phalanx
7	6, Warmblood, G	RF	Foot	Navicular bone fibrocartilage damage; distal navicular bone irregular; DSIL has severe damage including enthesiophytes at the origin and insertion; DDFT has pitting, fibrillation and altered structure of the dorsal surface at its insertion
8	7, Thoroughbred, F	RH	Fetlock	Open skin wound on the plantarolateral aspect of the fetlock region with thickening and haemorrhagic/oedematous soft tissues; lateral proximal sesamoid bone abnormal with abaxial loss of cortical bone; medulla, especially abaxially, has extensive bone loss with abaxial loss of cortical bone; medulla, especially abaxially, has extensive bone loss with osteonecrosis and oedema, fat necrosis, fibroplasia and spiculated bone fragments; bone abnormal at origin of lateral oblique distal sesamoidean ligament
9	7, Thoroughbred, G	RF	Foot	Severe navicular bone fibrocartilage and bone defect on midline in the distal third at site of adhesion to the DDFT; severe dorsal DDFT pathology; continued distal abnormality but easier to separate fibrinous/fibrous tissues between DDFT and DSIL; DSIL abnormal; marked synovial proliferation in navicular bursa; articular cartilage erosion on lateral condyle of distal aspect of middle phalanx
10	5, Hanoverian, G	RF	Foot	Navicular bone fibrocartilage abnormal; dorsal DDFT abnormal between navicular bone and insertion; CSL thickened and abnormal on palmar aspect; DSIL abnormal
		LF	Foot	Navicular bone fibrocartilage abnormal; dorsal DDFT abnormal at navicular bone and bursa; DSIL abnormal including enthesiophytes and the origin

CSL Collateral sesamoidean ligament, DDFT Deep digital flexor tendon, DSIL Distal sesamoidean impar ligament, F Female, G Gelding, LCL Lateral collateral ligament, LF Left forelimb, RF Right forelimb, RH Right hindlimb

for image acquisition; to image the foot and fetlock, modified solenoid coils shaped to fit the region were used. During the examinations the limbs were stabilised in a position to simulate that in a standing horse, using a wooden block and foam padding. To image the foot and pastern regions, sagittal plane images were aligned perpendicular to the dorsal aspect and parallel to the medial and lateral aspects of the second phalanx. Dorsal images were aligned parallel to the dorsal aspect of the second and distal phalanges. Transverse images were aligned perpendicular to the deep digital flexor tendon in the pastern region and in the region distal to the navicular bone; at the level of the navicular bone, transverse images were aligned perpendicular to the centre of the palmar border of the navicular bone. The limbs were re-frozen before being examined by high-field imaging.

The high-field images were acquired with a 1·5 T Signa Echospeed system (GE), using gradient echo and STIR sequences (Table 3). During image acquisition, the limbs were placed in the centre of a human extremity radiofrequency coil, as though in right lateral recumbency in a live horse, with the distal interphalangeal joint at an angle of between 170 and 190°C. Sagittal, dorsal and transverse images were aligned, as in the studies with the low-field system.

Pathological examination

Each limb was examined thoroughly by a pathologist unaware of the MRI findings, using a standard dissection protocol (Blunden and others 2006a, b), and the gross findings and abnormalities were recorded (Table 3) and a photographic record obtained. Samples from tissues with a suspected abnormality were prepared routinely, stained with haematoxylin and eosin, and examined microscopically as described by Blunden and others (2006a, b).

Image analysis

An offline workstation (Ultra 10; Sun microsystems) with dedicated software (GE Advantage Windows 3.1) was used to analyse the high-field images. The integrated image analysis features of the Hallmarq MRI scanner software running on a Windows XP workstation were used to analyse the low-field images. The definition and appearance of different structures and tissues were described for each type of image. The images from each limb were analysed by two trained analysts (both blinded to the results of the pathological examination and one blinded to each horse's history) for abnormalities, using a standard image-reading protocol to include the assessment of each tissue in a repeatable order for signal intensity and homogeneity, clarity of margins and relationships with other tissues.

Data analysis

A descriptive comparison of the appearance of the tissues on the high-field and low-field images was made to assist in understanding the relative appearance of the anatomical structures on the two MRI systems. A description of the pathological features of the abnormalities detected on the images was made to assist in determining the usefulness of each system for showing specific features. The findings on MRI were compared with the results of the pathological examinations to suggest which abnormalities were most clearly defined by each imaging technique.

Results

Positioning and plane of image acquisition

The appearance of some anatomical structures varied with the plane of the image and the position of the limb, due to the standing, extended position of the low-field images compared with the recumbent, flexed position of the high-field images. The structures affected included the deep digital flexor tendon (DDFT) and the collateral ligaments of the distal interphalangeal joint.

Appearance of images

In both the high-field and low-field images, the definition of tissue edges on both T2- and T2*-weighted images was less marked than on T1-weighted images. Some details of the tissues were less clear on low-field images, especially at the tissue margins, and there were some subtle differences in signal intensity within them. These were probably related to poorer resolution of the images, thicker slices and a difference in filtering level leading to smoothing of the images, and were not considered to be explained by differences in positioning.

Artefacts

Magic angle effect On T1-weighted high-field images, the magic angle effect led to increased signal intensity within the DDFT distal to the

TABLE 2: Parameters used in pulse sequences for imaging horses' limbs with a low-field MRI system

Pulse sequence	Plane	TE (ms)	TR (ms)	FE	PE	FOV (mm)	Slice thickness (mm)	Interslice spacing (mm)	Imaging options
Pilot	NA	7	62	150	120	220	7	NA	
STIR FSE	Sagittal/transverse	28	2910	340	175	175	5	1	No phase wrap
T1-weighted 3D HR	Sagittal/dorsal/transverse	8	23	340	130	170	2·5	0	
T1-weighted GRE HR	Sagittal/dorsal/transverse	8	92	384	192	170	3·5	0·7	Motion correction
T2*-weighted 3D HR	Sagittal/dorsal/transverse	13	32	384	192	170	2·5	0	
T2*-weighted GRE HR	Sagittal/dorsal/transverse	13	135	384	192	170	3·5	0·7	Motion correction
T2-weighted FSE	Sagittal/dorsal/transverse	84	2000	340	175	170	5	1	Motion correction

FE Frequency encoding, FOV Field of view, FSE Fast spin echo, GRE Gradient echo, HR High resolution, NA Not applicable, PE Phase encoding, STIR Short tau inversion recovery, TE Echo time, TR Repetition time

TABLE 3: Parameters used in pulse sequences for imaging horses' limbs with a low-field MRI system

Pulse sequence*	Plane	TE (ms)	TR (ms)	FE	PE	FOV (mm)	Slice thickness (mm)	Interslice spacing (mm)	Imaging options
3D SPGR	Sagittal	3·2	8·0	256	256	280	3	1·5	NPW, VBW, EDR, ZIP2, Zip512
3D T2* GRE	Sagittal	1·4	5·6	256	256	280	3	1·5	NPW, VBW, EDR, ZIP2, Zip512
STIR	Sagittal	25·4	10,500	256	192	220	4	1·0	VBW
3D SPGR	Dorsal	3·3	8·1	256	256	260	3	1·5	NPW, VBW, EDR, ZIP2, Zip512
3D T2* GRE	Dorsal	1·5	5·8	256	256	260	3	1·5	NPW, VBW, EDR, ZIP2, Zip512
STIR	Dorsal	24·8	5000	256	192	260	4	1·0	VBW
3D SPGR	Transverse	3·4	8·4	256	256	220	3	1·5	NPW, VBW, EDR, ZIP2, Zip512
3D T2* GRE	Transverse	1·4	5·8	256	192	220	3	1·5	NPW, VBW, EDR, ZIP2, Zip512
STIR	Transverse	25·3	10,500	256	192	220	4	1·0	VBW

* All 3D sequences used imaging options of variable band width (VBW), no phase wrap (NPW), extended dynamic range (EDR), zerofill interpolation processing (ZIP 512) to reconstruct the image to a 512/512 matrix and slice ZIP2 to double the number of reconstructed slices within the prescribed range. 2D sequences used variable band width. For the fast STIR sequence, an inversion time of 120 ms and echo train length of 4 were used

FE Frequency encoding, FOV Field of view, PE Phase encoding, TE Echo time, TR Repetition time

navicular bone, in the distal collateral sesamoidean ligament (CSL) and the distal sesamoidean impar ligament (DSIL) compared with the T1-weighted low-field images, where the structures had lower signal intensity. Some T1- and T2*-weighted images from the low-field system demonstrated asymmetry in signal intensity within the collateral ligaments of the distal interphalangeal joint and medial and lateral oblique sesamoidean ligaments. Repositioning the limb or using T2 fast spin echo scans produced images with a more symmetrical low signal intensity in both ligaments.

Partial volume effect The partial volume effect was more obvious on the low-field images, probably in association with the thicker slices and wider spacing between slices on these images.

Appearance of tissues

DDFT The normal DDFT had a uniform low signal intensity on T1-, T2- and T2*-weighted sequences. The high-field images showed some septal separation that was not clear on the low-field images. Distal to the navicular bone and near to the insertion there was increased signal intensity on the high-field images, which was most marked on T1-weighted images, but was absent on low-field images. The dorsal aspect of the DDFT was smooth and clearly separated from navicular bursal fluid on T2- and T2*-weighted images for both types of magnet.

Large tendon defects, core lesions or surface irregularity were clearly visible as increased signal intensity or a defect in the continuity of the tendon on both high- and low-field images of six limbs (Fig 1). Due to the different image orientation, the configuration of the lesion differed between the two systems for selected images on all the limbs, but the overall interpretation remained the same. Small focal lesions (approximately 1 mm diameter) visible on high-field images were not detected on low-field images of seven of the limbs. There was a tendency for focal increases in signal intensity on transverse high-field images to have better edge contrast and more variation in size between slices and a greater maximum intensity than on the low-field images. On low-field images these focal changes in intensity tended to be more gradual between the edge of the visible lesion and the adjacent tendon, with less variation in size between slices and a lower maximum intensity, probably as a result of partial volume effects. Subtle dorsal fibrillation at the level of the navicular bursa, including at the navicular bone and close to the insertion that was detectable on high-field images, was not clearly visible on low-field images of two limbs. Tendon splits were detectable on both high- and low-field images of three limbs. For some lesions, areas of poorly defined changes in structure on low-field images could be clearly defined by lesion type on high-field images (Fig 2). On T1-weighted images of the region between the distal navicular bone and the insertion, the magic angle effect in the high-field images made it more difficult to detect tendon splits or core lesions than on T1-weighted low-field images. However, on T2- and T2*-weighted images these lesions could be detected in both high- and low-field images.

Adhesions between the DDFT and the CSL, DSIL or navicular bone were detected on both low- and high-field images of four limbs, but they were more difficult to define in low-field images of one limb with an adhesion at the level of the distal navicular bone. Increased signal intensity on STIR images was detected in both high- and low-field images of four lesions, but one lesion involving the dorsal aspect of the insertion of the DDFT was easier to define on high-field images.

Ligaments The normal DSIL was easier to define on high-field images, especially in the transverse plane, and the contrast between the high signal intensity of the adjacent synovial fluid made the ligament clearer on T2- and T2*- than T1-weighted images from both systems. The DSIL on high-field T2-weighted images was a well-defined structure of low signal intensity, but on low-field images its appearance varied between a vague decrease in signal intensity and a more clearly defined structure of low signal intensity. The ability to visualise the DSIL better in cross-section (on transverse images) on high-field images appeared to relate to a difficulty in obtaining images at a consistent level on low-field images, probably due to the greater slice thickness and inter-slice spacing. However, it was possible to clearly define the DSIL in longitudinal orientation on low-field sagittal images. A rupture of the DSIL in one limb was visible on both high- and low-field images, as were bony irregularities at the origin or insertion, and a marked structural abnormality of the ligament, in four. However, in one limb, only high-field images gave a clear definition of enthesiophyte formation. Palmar irregularity was also observed only

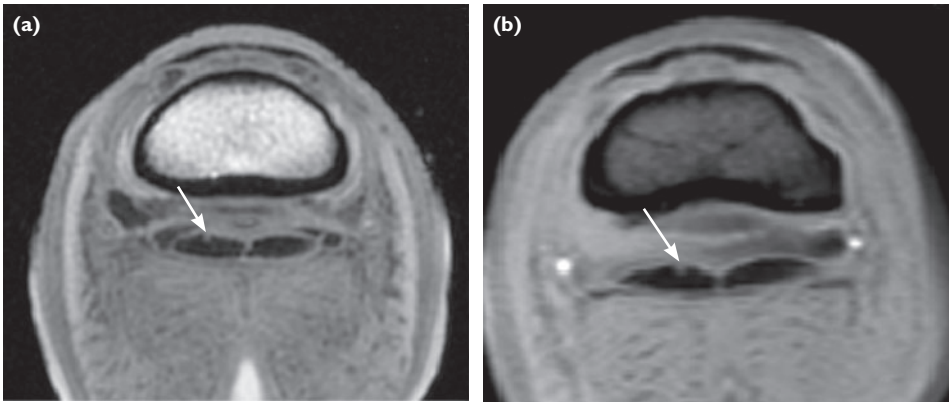

FIG 1: Comparison of (a) high-field (SPGR sequence) and (b) low-field (T1 GRE sequence) transverse images of the foot of horse 10, demonstrating a focal high lesion at the dorsal aspect of the medial lobe of the deep digital flexor tendon in the region just proximal to the navicular bone (arrow). Medial is to the left of the image

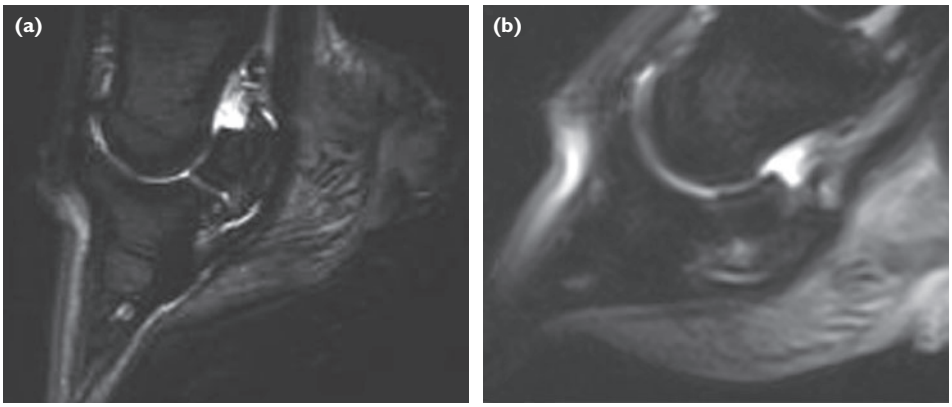

FIG 2: Comparison of (a) high-field (STIR sequence) and (b) low-field (STIR sequence) sagittal images of the foot of horse 7 with abnormalities in the deep digital flexor tendon (DDFT) and distal sesamoidean impar ligament (DSIL). A focal area of increased signal is visible in the DDFT close to its insertion into the distal phalanx, confirmed as a pathological change on gross examination. The signal intensity is slightly increased in the body of the DSIL, and markedly increased at its origin on the navicular bone and its insertion into the distal phalanx, in both the high- and low-field images. On pathological examination there was severe damage to the DSIL, particularly at its origin and insertion

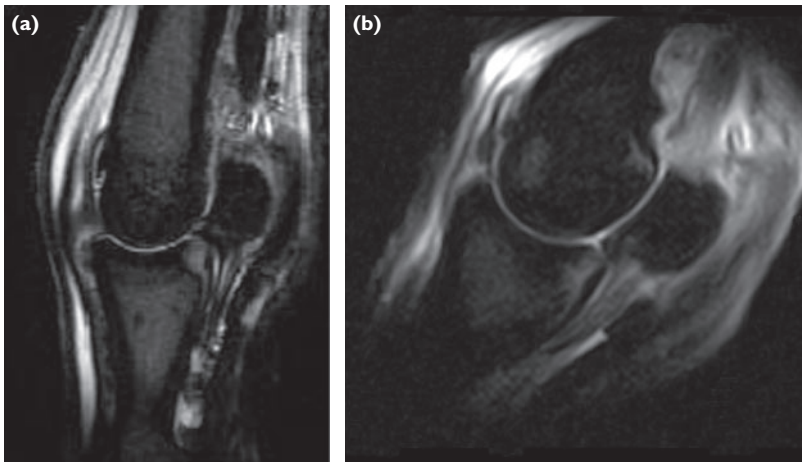

FIG 3: Signal intensity is high in STIR sequences in (a) high-field and (b) low-field images of the fetlock of horse 2 at the insertion of the cruciate distal sesamoidean ligaments (arrow)

on high-field images of four limbs. However, soft tissue interposed between the DSIL and the DDFT was detected easily by both systems, and this was present in all cases of palmar irregularity. When there was increased signal intensity at the origin and insertion of the DSIL on STIR images, it was clearly detectable by both systems (Figs 2, 3), even when it was more difficult to detect structural changes in the ligament on low-field images.

The normal CSL had a moderate signal intensity on T2-weighted high-field images but a low signal intensity on T2 and T2*-weighted low-field images. On T1-weighted high-field images the CSL had a moderate to high signal intensity (possibly related to the magic angle effect) and was less easy to define than on low-field images, in which the ligament had a lower signal intensity.

Adhesions between the CSL and the DDFT were detected on both high- and low-field images.

The normal DSL had better contrast with adjacent tissues on T2 and T2*-weighted than on T1-weighted high- and low-field images. Although T2- and T2*-weighted images of the oblique distal sesamoidean ligaments had a lower signal intensity than T1-weighted images, the ligaments had a slightly heterogeneous moderate signal intensity on both T1- and T2-weighted high-field images. No abnormalities were observed in the DSL of any of the limbs.

The normal collateral ligaments (CLs) of the proximal interphalangeal and metacarpophalangeal joints had a similar low signal density and appearance on high- and low-field T1-weighted, T2- and T2*-weighted and STIR images. The CLs of the distal interphalangeal joint had a low signal intensity on all sequences on high-field images, but there was some asymmetry in the signal intensity of T1- and T2*-weighted images when using the low-field system, attributed to the magic angle effect.

Enlargement or marked disruption of the CL was clearly detectable on both systems. Complete rupture of the metacarpophalangeal joint CL appeared on both systems as a loss of continuation of the ligament with slight widening of the remaining ligament proximal or distal to the rupture site, probably as a result of retraction, but with ragged edges (Fig 4). The partial rupture of two ligaments appeared as a partial disruption of the ligament, with local increased signal intensity of T2-weighted and STIR images but decreased signal intensity on T1-weighted images, suggesting an accumulation of fluid within the ligament.

Bone On T1-weighted images, normal bone had a clearly defined cortex and medulla in both the high- and low-field images. However, on the T2*-weighted images, the stronger T2 weighting on the low-field images made it more difficult to define the margin between the cortex and medulla than on the high-field images, in which the medulla had a higher signal intensity.

Marked bone disruption, cortical defects and changes in the medullary signal intensity were clearly evident on both systems (Fig 5). Moderate periosteal thickening and irregularity were clearly visible on both low- and high-field images. Low signal intensity on T1-weighted images and an increase in signal intensity on STIR images were visible in both systems. One 2 mm defect in the distal phalanx observed on high-field images was not detected on low-field images, but on T2-weighted images a distal metacarpal condylar fracture line was more clearly visible on the low-field than on the corresponding high-field image.

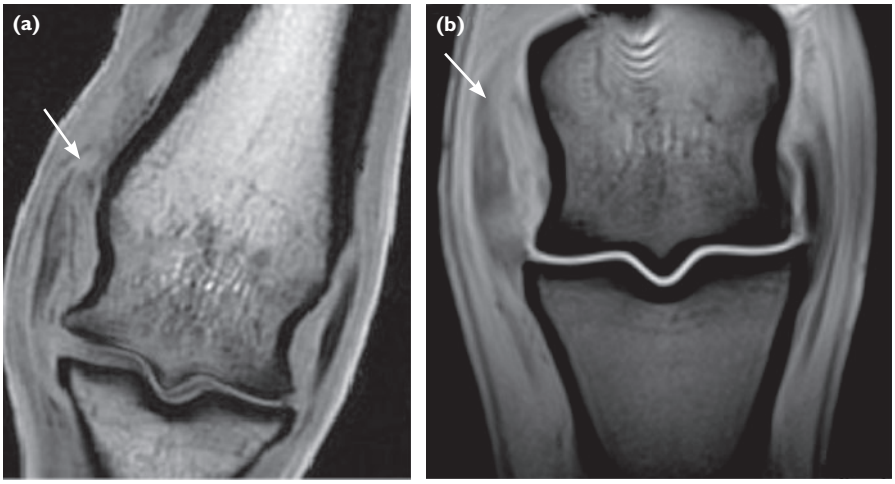

FIG 4: (a) High-field (SPGR sequence) and (b) low-field (GRE sequence) images, showing a complete rupture of the medial collateral ligament of the metacarpophalangeal joint of horse 2 (arrow). The rupture is visible as a loss of continuity, increased signal intensity and disruption of local anatomy in both images. Medial is to the left of the images

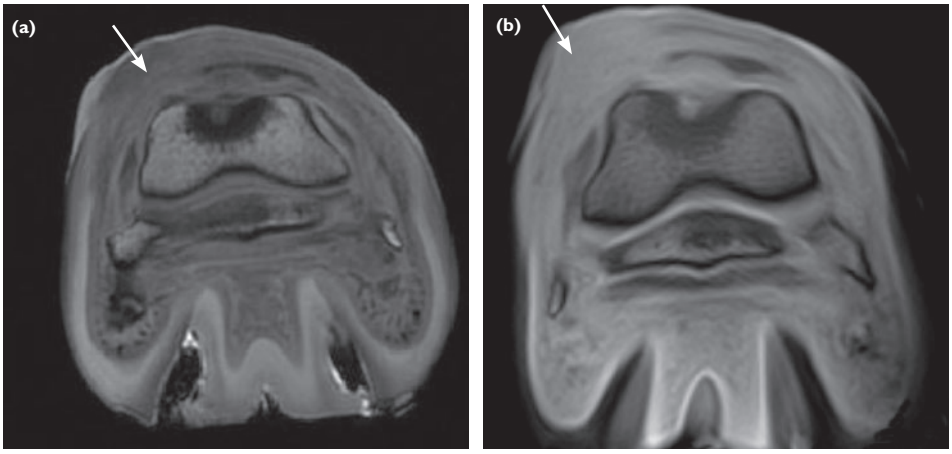

FIG 5: (a) High-field (SPGR sequence) and (b) low-field (T1 GRE sequence) transverse images of the foot of horse 3, showing damage to the dorsal aspect of the middle phalanx, common digital extensor tendon and overlying soft tissues. Both images clearly show swelling and increased signal intensity of the dorsal soft tissues to the left of the image (arrow). There is a large area of low signal intensity in the dorsal medulla of the middle phalanx surrounding a focal area of high signal intensity involving the dorsal cortex; both the high- and low-field images are oblique images, so that the size and shape of the collateral ligaments of the distal interphalangeal joint and osseous structures are different on medial and lateral sides

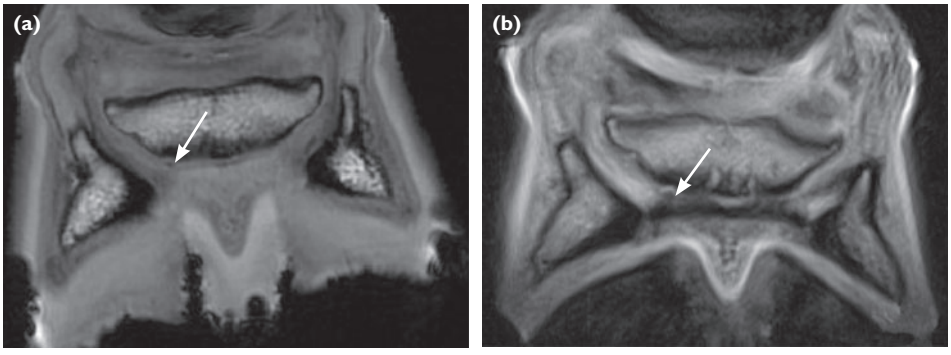

FIG 6: (a) High-field (SPGR sequence) and (b) low-field (T1 GRE sequence) dorsal images showing fragmentation (arrow) of the distal border of the navicular bone of horse 7

In the navicular bone, mild endosteal irregularity of the flexor border was easily detectable on high-field T1- and T2-weighted images of three of the limbs. On low-field images, endosteal irregularity was more easily detectable on T2- than T1-weighted images, but mild changes were less clearly defined than on the high-field images for two of the three limbs. Abnormalities of the flexor surface of the navicular bone, including an irregularity of the flexor subchondral bone, a flexor subchondral bone defect or an accumulation of fluid palmar to the bone, were detected on both high- and low-field systems, but these abnormalities were more clearly defined on the high-field images. Increased signal intensity on STIR was clearly evident on both high- and low-field images, particularly extending as a band-shaped signal from the insertion of the CSL to the origin of the DSIL in seven of the limbs. Distal border fragments were visible on both systems, and were especially obvious on dorsal/frontal plane images (Fig 6).

In horse 5, there was no fat signal in the medulla, giving the appearance of fat suppression on all the images except the STIR images, in which there was a high signal intensity in the medulla, suggesting that the marrow fat had been replaced by fluid.

Articular cartilage On both high- and low-field images normal articular cartilage gave a moderate signal intensity, with higher intensity on T1- than T2-weighted images. The cartilage surface was most clearly defined when adjacent to the contrast of synovial fluid. On high-field images it was possible to separate the proximal and distal articular surfaces in all the joints examined. However, on low-field images the cartilage from each articular surface was visible separately only at the joint margins, and for most of the joint surface the cartilage appeared as a single continuous line (Fig 7).

Irregularities of the cartilage surface were clearly visible on high-field images, in which the two articular surfaces could be seen as separate layers in six limbs, but these defects were detected on low-field images in only two limbs (Fig 8). When there were concurrent changes in the subchondral bone, they were visible on both high- and low-field images, in three of the limbs.

Synovium, synovial fluid and periarticular tissues Normal synovial fluid and spaces were clearly evident on T2-weighted high-field images, but the synovial fluid pouches of the navicular bursa and the distal interphalangeal joint were more difficult to visualise on low-field images. On T2-weighted images the joint capsule had a lower signal intensity on low-field than on high-field images.

Chronic synovial proliferation in the navicular bursa was visible in both high- and low-field images, replacing the low signal intensity of the synovial fluid on T1-weighted images and the high signal intensity on T2-weighted images. In two cases, thickening, disruption or rupture of the joint capsule with changes in signal intensity were easily detected on both systems. In one case, disruption, fluid accumulation, with increased signal intensity on T2-weighted images, and swelling of periarticular soft tissues were observed on both systems. In horse 5, there was an absence of the expected fat signal in the palmar soft tissues with both MRI systems, and it was apparently replaced in the digital cushion by a fluid signal, probably related to emaciation.

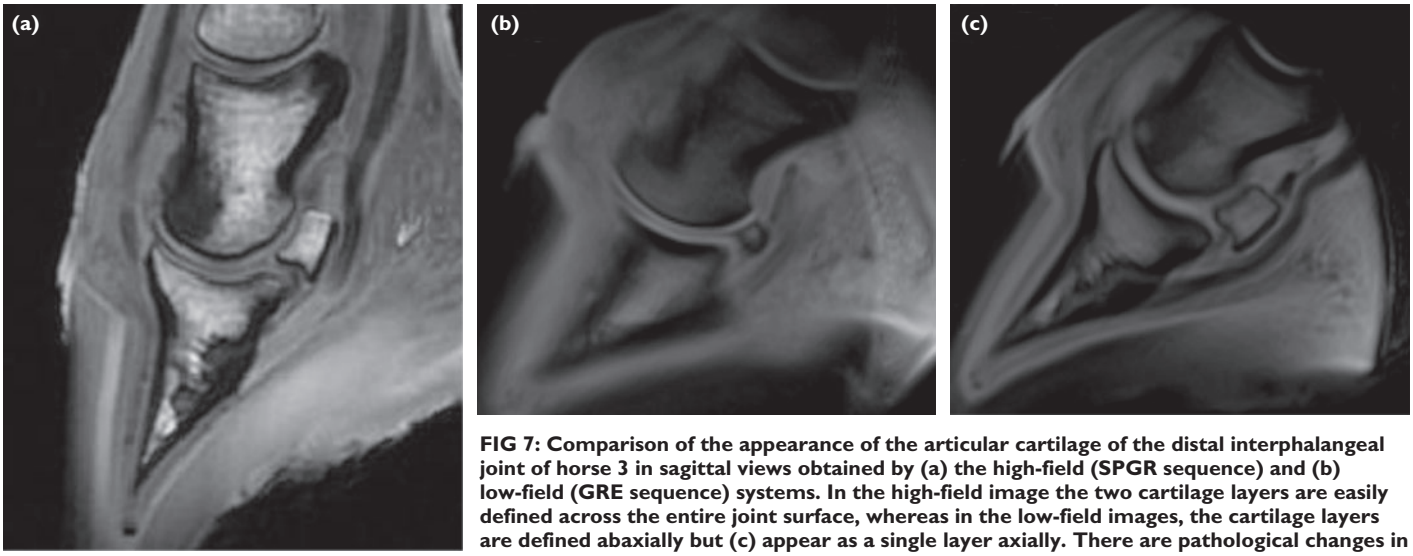

FIG 7: Comparison of the appearance of the articular cartilage of the distal interphalangeal joint of horse 3 in sagittal views obtained by (a) the high-field (SPGR sequence) and (b) low-field (GRE sequence) systems. In the high-field image the two cartilage layers are easily defined across the entire joint surface, whereas in the low-field images, the cartilage layers are defined abaxially but (c) appear as a single layer axially. There are pathological changes in the dorsal aspect of the middle phalanx and overlying soft tissues on both the high and low-field images

Laminae Normal laminal layers were clearly defined on T1-weighted low- and high-field images. The laminar layers were visible on the high-field T2*-weighted images, but on the low-field images the epidermis was so hypointense that it could not be defined and the deep laminar layers were relatively very hyperintense and difficult to separate.

In one limb, small gas pockets could be clearly defined within the laminae on both high- and low-field images, and the laminae appeared irregular.

Detection of lesions on MRI

All the ligaments (CL, DSIL, DSL, CSL and intersesamoidean ligament) and tendons (CDE, SDFT and DDFT) that were normal on gross pathological examination were classified as normal on MRI. All the tendons and ligaments that were abnormal on pathological examination were classified overall as abnormal on both high- and low-field MRI. However, details of the lesions, including small focal lesions, were clearer on the high-field images. All the bone abnormalities detected on gross examination were detected as abnormal on MRI, but some detailed aspects of the lesions were clearer on high-field images. Articular cartilage that was normal on gross pathological examination was also classified as normal on MRI, but only high-field MRI detected all the articular cartilage lesions detected by pathological examination. An abnormality was detected on MRI of all the limbs that had grossly abnormal navicular flexor fibrocartilage on pathological examination. Lesions of the synovium, joint capsule and periarticular tissues identified by gross pathological examination were detected on MRI. None of the limbs that were normal on gross examination were classified as abnormal on either high- or low-field images.

Discussion

This study has limitations because only limbs from dead horses with severe pathological changes were examined by the two MRI systems. The effects of movement could not be evaluated, and more subtle (but clinically significant) lesions could not be evaluated.

Nevertheless, the results of the study indicate that the majority of structures and abnormalities in the distal limbs can be detected by both high-field MRI (which in live horses is performed under general anaesthesia) and low-field MRI (which in live horses is most often performed under standing sedation). Both systems gave results broadly in agreement with the findings of pathological examinations. However, there were differences between the two systems in the details of the images acquired and in their ability to detect more subtle lesions. The major advantages of the low-field system in clinical practice include lower installation and maintenance costs, and the ability to image a standing horse. However, the low-field system has disadvantages. In general, the signal-to-noise ratio, contrast and resolution increase with the field strength (Ghazinoor and others 2007), and the major disadvantages of low-field scanners is their poorer image resolution; this disadvantage was apparent in this study. However, most of the anatomical structures and most of the lesions in the cadaver limbs examined were clearly identified by both systems, which suggests that either system could yield images of diagnostic quality.

The differences in the appearance of the images between the systems were largely determined by the selection of imaging parameters, differences in the size of the field of view and different acquisition angles. The field of view in the high-field system was considerably larger, and two or three fields of view were required in the low-field system to cover the same area. Under general anaesthesia, the limbs are positioned with the metacarpophalangeal, proximal and distal interphalangeal joints in flexion, which was evident in the high-field images, in contrast to the extension of these joints in the low-field images (as would be the case in a standing horse). This resulted in differences in the anatomical arrangement and appearance of images taken by the two systems.

Compared with high-field systems, it is more difficult to maintain the signal-to-noise ratio in a low-field system without increasing the pixel size, slice thickness or acquisition time, changes that limit the capacity to improve the resolution and quality of the images within the same acquisition time. Lower resolution and increased slice thickness are likely to increase the partial volume effect, which could be why the margins of some lesions were less clearly defined on the low-field system, and some small lesions were not detected. The level of filtering could also have influenced the detection of small tissue defects.

There were differences in the appearance of the DDFT, CSL, distal interphalangeal joint CL and oblique sesamoidean ligaments between the two systems that were attributed to magic angle effects. In the high-field system, the static magnetic field is orientated longitudinally with the limb, whereas in the low-field system it is orientated transversely across the limb. In the high-field system, a magic angle artefact has been recognised in the DDFT distal to the navicular bone (Busoni and Snaps 2002, Murray and others 2004, 2006b), and the DSIL and parts of the CSL (Murray and others 2006b). In low-field systems with a transverse static magnetic field, magic angle effects have been described within the distal interphalangeal collateral ligaments (Spriet and others 2007, Smith and others 2008). It is therefore important that pulse sequences with a long echo time are used to assess these structures. Alternatively, reducing the flip angle in gradient echo sequences reduces magic angle effects (Zurlo and others 2000).

The appearance of normal tissues was very similar with the two systems, but it was possible to define small structures more clearly on the high-field images. It was difficult to visualise the DSIL on low-field images, and irregular margins of the DSIL were seen only on high-field images. However, all the cases with irregular margins of the DSIL also

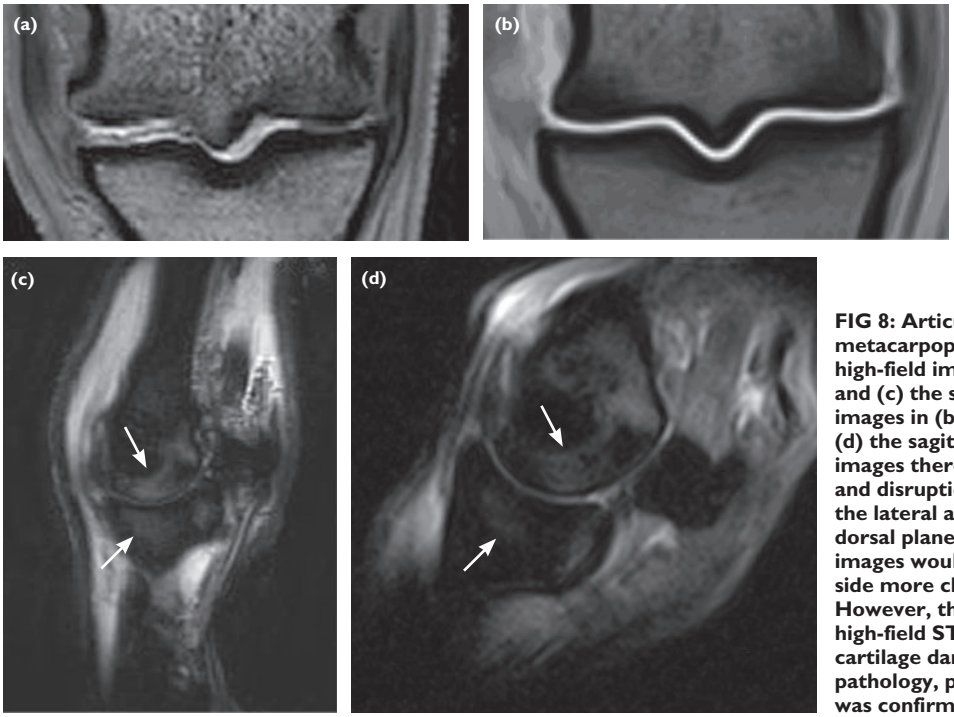

FIG 8: Articular cartilage damage in the metacarpophalangeal joint of horse 2. Comparison of high-field images in (a) the dorsal plane (SPGR sequence) and (c) the sagittal plane (STIR sequence) with low-field images in (b) the dorsal plane (T1 GRE sequence) and (d) the sagittal plane (STIR sequence). On the high-field images there is evidence of cartilage surface irregularity and disruption on the medial aspect with cartilage loss on the lateral aspect, which is not evident on the low-field dorsal plane image, although it is possible that low-field images would have shown joint collapse on the lateral side more clearly under weight-bearing conditions. However, the increased signal intensity on the low and high-field STIR images (arrows) in the region of the cartilage damage indicates the presence of osteochondral pathology, probably secondary to joint instability, which was confirmed on pathological examination

had accumulations of soft tissue in the navicular bursa between the DDFT and DSIL, and these were detected on low-field images, suggesting that on low-field images they could be used as an indicator of possible DSIL damage. In addition, increased signal density on STIR images at the origin and insertion of the DSIL was detected on both systems and can be a good indicator of DSIL damage (Murray and Dyson 2007).

Both high- and low-field MRI detected the presence or absence of macroscopic pathological changes in tendon, ligament, bone and other soft tissues, but high-field MRI sometimes detected small lesions or made the configuration of the lesions clearer in relation to the pathological findings. High-field imaging was able to detect abnormalities of articular cartilage that were undetectable in the low-field images if the articular surfaces were closely apposed and there was no concurrent subchondral bone damage. Lesions of articular cartilage near the margin of a joint or in a region where the two joint surfaces were separated, for example, between the condyles of the middle phalanx, were generally detectable by both systems. It is therefore important to consider the potential limitation of low-field standing images for the detection of damage to articular cartilage in the absence of subchondral bone pathology. In a standing live horse, loading would be likely to increase the area of contact between the articular surfaces and therefore potentially exacerbate the problem, unless there was complete loss of cartilage from an area, when a reduced joint space might be apparent.

Most studies that have compared high-field and low-field MRI in human musculoskeletal disease have reported comparable diagnostic accuracy (Martí-Bonmatí and Kormano 1997). For example, it has been shown that low-field MRI is an acceptable technique for the diagnosis of lesions of the shoulder, with diagnostic accuracy similar to that obtained with high-field scanners (Merl and others 1999, Tung and others 2000, Shellock and others 2001, Zlatkin and others 2004). However, in one comparative study lesions were identified by high-field but not low-field MRI in nine of 40 patients, which led to a significant change in patient management (Magee and others 2003). However, that study was limited because the low-field studies had a limited spatial resolution that may have reduced the ability to see abnormalities secondary to volume averaging (Ghazinoor and others 2007). Furthermore, studies comparing the results of MRI of the human knee with the results of surgery, and/or comparing the results of high-field and low-field MRI, have generally observed only small differences in the sensitivities and specificities of the two systems for the diagnosis of meniscal and anterior cruciate lesions (Barnett 1992, Kinnunen and others 1994, Kladny and others 1995, Vallet and others 1995, Rutt and Lee 1996, Franklin and others 1997, Riel and others 1999, Cotten and others 2000, Oei and others 2003, Cevokol and others 2004). However, even with high-field scanners, it is difficult to resolve images of articular cartilage (Woertler and others 2000, Kneeland and Reddy 2001, Tavernier and Cotton 2005).

The results of this study suggest that both high-field and low-field MRI gave comparable data about most of the anatomical structures and major pathological lesions in the limbs of these 10 horses. Both systems are likely to become important diagnostic techniques in the evaluation of lameness in horses, in the same way that they have become important techniques in the evaluation of musculoskeletal disorders in human beings. However, high-field scanners produce images with better resolution that may provide greater diagnostic accuracy for certain lesions in some structures, such as articular cartilage. Further studies are required to assess the sensitivity and specificity of MRI in live horses for the diagnosis of particular lesions in the distal limb. In addition, the imaging parameters and radiofrequency coils need to be developed to improve the accuracy of the diagnosis of articular cartilage damage and other specific lesions by MRI.

Acknowledgements

The authors thank Carolyne Tranquille and Julie Breingan for assisting with the acquisition of the high-field images and Ray Wright for the histological preparations.

References

ADAMS, O. R. (1957) Veterinary notes on lameness and shoeing of horses. Dissertation. Colorado State University

BARNETT, M. (1992) MR diagnosis of internal derangements of the knee: effect of field strength on efficacy. *American Journal of Roentgenology* **161,** 115-118

BLUNDEN, A., DYSON, S., MURRAY, R. & SCHRAMME, M. (2006a) Histopathology in horses with chronic palmar foot pain and age-matched controls. Part 1: navicular bone and related structures. *Equine Veterinary Journal* **38,** 15-22

BLUNDEN, A., DYSON, S., MURRAY, R. & SCHRAMME, M. (2006b) Histopathology in horses with chronic palmar foot pain and age-matched controls. Part 2: the deep digital flexor tendon. *Equine Veterinary Journal* **38,** 23-27

BOADO, A., KRISTOFFERSEN, M., DYSON, S. & MURRAY, R. (2005) The use of nuclear scintigraphy and magnetic resonance imaging to diagnose chronic penetrating wounds in the equine foot. *Equine Veterinary Education* **17,** 62-68

BUSONI, V. & SNAPS, F. (2002) Effect of deep digital flexor tendon orientation on magnetic resonance imaging signal intensity in isolated equine limbs – the magic angle effect. *Veterinary Radiology & Ultrasound* **43,** 428-430

CEVOKOL, C., KARAALI, K., ESEN, G., APAYDIN, A., OZENCI, M. & SENOL, U.

(2004) MR imaging of meniscal tears at low-field (0·35T) and high-field (1·5T) MR units. *Tanısal ve Girişimsel Radyokoji* **10,** 316-319

COTTEN, A., DEFAULT, E., DEMONDION, X., LAPÈGUE, F., BOUKHELFIA, M., BOUTRY, N., CHASTANET, P. & GOUGEON, F. (2000) MR imaging of the knee at 0·2 and 1·5 T: correlation with surgery. *American Journal of Roentgenology* **174,** 1093-1097

DYSON, S., BLUNDEN, T. & MURRAY, R. (2008) The collateral ligaments of the distal interphalangeal joint: magnetic resonance imaging and post mortem observations in 25 lame and 12 control horses. *Equine Veterinary Journal* **40,** 538-544

DYSON, S. & MURRAY, R. (2004) Collateral desmitis of the distal interphalangeal joint of 62 horses. *Proceedings of the American Association of Equine Practitioners* **50,** 248-256

DYSON, S. J., MURRAY, R. & SCHRAMME, M. C. (2005) Lameness associated with foot pain: results of magnetic resonance imaging in 199 horses (January 2001-December 2003) and response to treatment. *Equine Veterinary Journal* **37,** 113-121

DYSON, S., MURRAY, R., SCHRAMME, M. & BRANCH, M. (2003a) Magnetic resonance imaging of the equine foot: 15 horses. *Equine Veterinary Journal* **35,** 18-26

DYSON, S. J., MURRAY, R., SCHRAMME, M. & BRANCH, M. (2004) Collateral desmitis of the distal interphalangeal joint in 18 horses (2001-2002). *Equine Veterinary Journal* **36,** 160-166

DYSON, S., MURRAY, R., SCHRAMME, M. & BRANCH, M. (2003b) Lameness in 46 horses associated with deep digital flexor tendonitis in the digit: diagnosis confirmed with magnetic resonance imaging. *Equine Veterinary Journal* **35,** 681-690

FRANKLIN, P. D., LEMON, R. A. & BARDEN, H. S. (1997) Accuracy of imaging the menisci on an in-office, dedicated, magnetic resonance imaging extremity system. *American Journal of Sports Medicine* **25,** 382-388

GHAZINOOR, S., CRUES, J. V., III & CROWLEY, C. (2007) Low-field musculoskeletal MRI. *Journal of Magnetic Resonance Imaging* **25,** 234-244

KINNS, J. & MAIR, T. (2005) The use of magnetic resonance imaging to assess soft tissue damage in the foot following penetrating injury in 3 horses. *Equine Veterinary Education* **17,** 69-73

KINNUNEN, J., BONDESTAM, S., KIVIOJA, A., AHOVUO, J., TOIVAKKA, S. & TULIKOURA, I. (1994) Diagnostic performance of low field MRI in acute knee injuries. *Magnetic Resonance Imaging* **12,** 1155-1160

KLADNY, B., GLÜCKERT, K., SWOBODA, B., BEYER, W. & WESELOH, G. (1995) Comparison of low-field (0·2 Tesla) and high-field (1·5 Tesla) magnetic resonance imaging of the knee joint. *Archives of Orthopaedic and Trauma Surgery* **114,** 281-286

KNEELAND, J. & REDDY, R. (2007) Frontiers in musculoskeletal MRI: articular cartilage. *Journal of Magnetic Resonance Imaging* **25,** 339-344

KRISTOFFERSEN, M., DYSON, S., MURRAY, R., SCHRAMME, M. & LAMA, A. (2004) Magnetic resonance imaging and scintigraphic findings in 5 horses with obscure foot lameness associated with penetrating injuries. *Proceedings of the American Association of Equine Practitioners* **50,** 320-327

MAGEE, T., SHAPIRO, M. & WILLIAMS, D. (2003) Comparison of high-field-strength versus low-field-strength MRI of the shoulder. *American Journal of Roentgenology* **181,** 1211-1251

MAIR, T. & KINNS, J. (2005) Deep digital tendonitis in the equine foot diagnosed by magnetic resonance imaging in the standing patient: 18 cases. *Veterinary Radiology & Ultrasound* **46,** 458-466

MAIR, T., KINNS, J. & BOLAS, N. (2003) Magnetic resonance imaging of the distal limb of the standing horse: technique and review of 40 cases of foot lameness. *Proceedings of the American Association of Equine Practitioners* **49,** 29-41

MAIR, T., KINNS, J., JONES, R. & BOLAS, N. (2005) Magnetic resonance imaging of the distal limb of the standing horse. *Equine Veterinary Education* **17,** 74-78

MARTÍ-BONMATÍ, L. & KORMANO, M. (1997) MR equipment acquisition strategies: low-field or high-field scanners. *European Radiology* **7** (Suppl 5), 263-268

MERL, T., SCHOLZ, M., GERHARDT, P., LANGER, M., LAUBENBERGER, J., WEISS, H. D., GEHL, H. B., WOLF, K. J. & OHNESORGE, I. (1999) Results of a prospective multicentre study for evaluation of the diagnostic quality of an open whole-body low-field MRI unit. A comparison with high-field MRI measured by the applicable gold standard. *European Journal of Radiology* **30,** 43-53

MURRAY, R. C., BLUNDEN, T. S., SCHRAMME, M. C. & DYSON, S. J. (2006a) How does magnetic resonance imaging represent histologic findings in the equine digit? *Veterinary Radiology & Ultrasound* **47,** 17-31

MURRAY, R. & DYSON, S. (2007) Image interpretation and artifacts. *Clinical Techniques in Equine Practice* **6,** 16-25

MURRAY, R. & MAIR, T. (2005) Use of magnetic resonance imaging in lameness diagnosis in the horse. *In Practice* **27,** 70-78

MURRAY, R. C., ROBERTS, B. L., SCHRAMME, M. C., DYSON, S. J. & BRANCH, M. (2004) Quantitative evaluation of equine deep flexor tendon morphology using magnetic resonance imaging. *Veterinary Radiology & Ultrasound* **45,** 103-111

MURRAY, R. C., SCHRAMME, M. C., DYSON, S. J., BRANCH, M. V. & BLUNDEN, T. S. (2006b) Magnetic resonance imaging characteristics of the foot in horses with palmar foot pain and control horses. *Veterinary Radiology & Ultrasound* **47,** 1-16

OEI, E. H., NIKKEN, J. J., VERSTIJNEN, A. C., GINAI, A. Z. & MYRIAM HUNINK, M. G. (2003) MR imaging of the menisci and cruciate ligaments: a systematic review. *Radiology* **226,** 837-848

RIEL, K. A., REINISCH, M., KERSTING-SOMMERHOFF, B., HOF, N. & MERL, T. (1999) 0·2-Tesla magnetic resonance imaging of internal lesions of the knee joint: a prospective arthroscopically controlled clinical study. *Knee Surgery, Sports Traumatology, Arthroscopy* **7,** 37-41

ROSS, M. W. (2003) Diagnosis of lameness. In Diagnosis and Management of Lameness in the Horse. Eds M. W. Ross, S. J. Dyson. W. B. Saunders. p 4

RUTT, B. K. & LEE, D. H. (1996) The impact of field strength on image quality in MRI. *Journal of Magnetic Resonance Imaging* **6,** 57-62

SCHNEIDER, R., GAVIN, P. & TUCKER, R. (2003) What MRI is teaching us about navicular disease. *Proceedings of the American Association of Equine Practitioners* **49,** 210-219

SCHRAMME, M., MURRAY, R., BLUNDEN, A. & DYSON, S. (2005) A comparison between MRI, pathology and radiology in 34 limbs with navicular syndrome and 25 control limbs. *Proceedings of the American Association of Equine Practitioners* **51,** 348-358

SCHRAMME, M., MURRAY, R., DYSON, S., WHITTON, C., BUCKLEY, C., WALES, A. & AL, E. (2001) Experiences with the use of MRI in equine orthopaedics. Proceedings of the BEVA Spring meeting. Sutton Coldfield, March 7, 2001. pp 17-18

SHELLOCK, F. G., BERT, J. M., FRITTS, H. M., GUNDRY, C. R., EASTON, R. & CRUES, J. V., 3rd (2001) Evaluation of the rotator cuff and glenoid labrum using a 0·2-Tesla extremity magnetic resonance (MR) imaging system: MR results compared to surgical findings. *Journal of Magnetic Resonance Imaging* **14,** 763-770

SHERLOCK, C. E., KINNS, J. & MAIR, T. S. (2007) Evaluation of foot pain in the standing horse by magnetic resonance imaging. *Veterinary Record* **161,** 739-744

SMITH, M. A., DYSON, S. J. & MURRAY, R. C. (2008) Is a magic angle effect observed in the collateral ligaments of the distal interphalangeal joint or the oblique sesamoidean ligaments during standing magnetic resonance imaging? *Veterinary Radiology & Ultrasound* **49,** 509-515

SPRIET, M., MAI, W. & MCKNIGHT, A. (2007) Asymmetric signal intensity in normal collateral ligaments of the distal interphalangeal joint in horses with a low-field MRI system due to the magic angle effect. *Veterinary Radiology & Ultrasound* **48,** 95-100

TAVERNIER, T. & COTTEN, P. (2005) High- versus low-field MR imaging. *Radiological Clinics of North America* **43,** 673-681

TUNG, G. A., ENTZIAN, D., GREEN, A. & BRODY, J. M. (2000) High-field and low-field MR imaging of superior glenoid labral tears and associated tendon injuries. *American Journal of Roentgenology* **174,** 1107-1114

VALLET, A. D., LEE, D. H., MUNK, P. L., HEWETT, L., ELIASZIW, M., VIDITO, L., DUNLAVY, S., VIDITO, L., FOWLER, P. J., MINIALI, A. & AMENODLA, A. (1995) Anterior cruciate ligament tear: prospective evaluation of diagnostic accuracy of middle- and high-field-strength MR imaging at 1·5 and 0·5 Tesla. *Radiology* **197,** 826-830

WOERTLER, K., STROTHMANN, M., TOMBACH, B. & REIMER, P. (2000) Detection of articular cartilage lesions: experimental evaluation of low- and high-field-strength MR imaging at 0·18 and 1·0T. *Journal of Magnetic Resonance Imaging* **11,** 678-685

ZLATKIN, M. B., HOFFMAN, C. & SHELLOCK, F. G. (2004) Assessment of the rotator cuff and glenoid labrum using an extremity MR system: MR results compared to surgical findings from a multi-centre study. *Journal of Magnetic Resonance Imaging* **19,** 623-663

ZUBROD, C. J., FARNSWORTH, K. D., TUCKER, R. L. & RAGLE, C. A. (2005) Injuries of the collateral ligaments of the distal interphalangeal joint diagnosed by magnetic resonance. *Veterinary Radiology & Ultrasound* **46,** 11-16

ZUBROD, C. J., SCHNEIDER, R. K., TUCKER, R. L., GAVIN, P. R., RAGLE, C. A. & FARNSWORTH, K. D. (2004) Use of magnetic resonance imaging for identifying subchondral bone damage in horses: 11 cases (1999-2003). *Journal of the American Veterinary Medical Association* **224,** 411-418

ZURLO, J. V., BLACKSIN, M. F. & KARIMI, S. (2000) The influence of flip angle on the magic angle effect. *Skeletal Radiology* **29,** 593-596